Automated vial defect inspection using Gabor wavelets and k-means clustering

Vishwanatha C. R.[1], V. Asha[2], Channabasava[1], Sreekanth Rallapalli[1]
[1]Department of Master of Computer Applications, Nitte Meenakshi Institute of Technology, Nitte (Deemed to be University),
Bengaluru, India
[2]Department of Master of Computer Applications, New Horizon College of Engineering, Bengaluru, India

Article Info	ABSTRACT
	This study proposes a machine vision-based defect inspection system for pharmaceutical vials, aiming to ensure the quality and safety of medicinal fluids. The system employs a series of image processing techniques, including denoising, feature extraction using the Gabor wavelet transform, segmentation, clustering with the K-means algorithm, and precise defect identification using the Canny edge operator. Experimental results demonstrate high performance, with recall, precision, accuracy, and F1-score exceeding 98%. Additionally, the proposed method achieves area under the curve-receiver-operating characteristic curve (AUC-ROC) and AUC-precision-recall (PR) values of approximately 98%. The system's average computational time is 355 microseconds, indicating its potential for real-time defect detection. Overall, this approach offers an effective solution for identifying various cosmetic defects such as scratches, bruises, cracks, and black spots, in pharmaceutical vials without the need for vial classification training.

Corresponding Author:

V. Asha
Department of Master of Computer Applications, New Horizon College of Engineering
Bengaluru-560103, Karnataka, India
Email: asha.gurudath@gmail.com

1. INTRODUCTION

Safe, high-quality vials are vital for maintaining sterile conditions and preserving medicine integrity in pharmaceuticals. They shield fluids from contamination, leaks, and degradation. Advanced inspection methods like machine vision, optical inspection, and automated defect detection ensure compliance with quality standards like good manufacturing practices (GMP) and good laboratory practices (GLP). By leveraging technology, these methods detect subtle defects, enabling corrective actions and preventing defective vials from entering the market. Evolving quality assurance (QA) protocols and technology integration, particularly machine learning (ML) with computer vision (CV), enhance pharmaceutical container reliability and safety by identifying issues like cracks, black spots, scratches, and bubbles. Figure 1 shows a typical vial used in pharmaceutical packing.

Figure 1. Commonly used pharmaceutical vial

Various methodologies have been applied to detect flaws in glass vials and bottles. The low-angle and large divergence angle (LALDA) vision system [1] enhances pharmaceutical bottle cap inspection by improving defect contrast and mitigating overexposure, addressing occlusions and inconsistent illumination. using HSV-based multi-channel segmentation (MCS), it achieves over 95% accuracy. X-ray-based inspection system [2] detects non-metallic contaminants but relies on costly defective samples. This study achieves 97.4% accuracy for glass fragments, improving sensitivity to 1.0 and F1-score to 0.980. Heuristic segmentation for vial defect detection [3] showed high accuracy but required validation on larger datasets. Farhangi *et al*. [4] proposed a thresholding-based system for detecting cap defects, seal integrity, and liquid level variations in edible oil and beverage bottles, achieving 95.6% accuracy using a complementary metal oxide semiconductor (CMOS) camera. However, worn labels and weak seals pose challenges. Liu *et al*. [5] achieved more than 98% accuracy in detecting vial defects, but faced challenges in adapting to different lighting conditions. The black top-hat transform algorithm [6] combined with hybrid image processing addressed localization issues but had high computational costs, impacting real-time deployment. Other approaches, such as Canny edge detection [7] and clustering methods [8], performed well but struggled with specific defects, while advanced multiview systems [9] encountered segmentation challenges due to uneven lighting. Plastic bottle defect detection [10] presented challenges with data and computational needs, while zonal and time-sharing computational imaging (ZTSCI) techniques [11] laid a foundation for gray image flaw detection. Convolutional neural networks (CNNs) and deep learning models [12], [13] improved detection capabilities on large datasets, while field-programmable gate array (FPGA)-based systems [14] accelerated bottle cap inspection, though still faced server strain.

Xu *et al*. [15] proposed a defect detection system for filled vials that integrates traditional image processing and deep learning. Defect detection of surface and contents in vials (DDSCNet), built on YOLOv8 with quadra fusion and attention (QUFUAtt) for feature fusion, ACmix for defect focus, and linear deformable convolution for weak feature extraction, achieves 76.7% mAP on VialG1_DET, 65.9% on VialG2_DET, and 86.9% on VialG3_DET with 9.3 GFLOPS, outperforming YOLOv11 by 3.5%. YOLO-based models [16]–[22] demonstrated efficient defect detection across different surfaces, but some struggled with small targets or high computational costs. Lastly, methods using robotic technologies and AI [23], [24] enhanced inspection accuracy, though challenges with sensor calibration and scalability persisted. The proposed study addresses these gaps by aiming for comprehensive defect detection across the entire vial surface, enhancing reliability without relying on complex deep learning architectures. The curated dataset tailored for vial defect inspection overcomes limitations seen in existing methods.

The motivation for using Gabor wavelets is their ability to detect vial defects via machine vision without human intervention [25]. In this study, Gabor wavelets denoise and extract vial image features, which are then segmented by the K-means clustering algorithm based on feature similarities. The Canny edge operator highlights defects across the vial's surface, neck, top, and bottom with high precision. Python, along with the scikit image library, is used for implementation. Key features of the method include its applicability to any defect in any vial region, making it highly versatile. It does not require a training stage or defect-free samples, thereby eliminating the need for thresholding. The defect detection process is fully automated through K-means clustering, allowing for the specific detection of various defects such as scratches, bubbles, and cracks, rather than merely categorizing vials.

The paper is organized in the following way: section 2 briefly explains the proposed model for defect detection using Gabor wavelets and K-means clustering. Section 3 presents experiment on various real defective vial images. The conclusions are discussed in section 4.

2. METHOD

Machine vision is used in place of human vision to detect defects using computer algorithms and processors. The proposed machine vision system comprises four steps. First, an image is acquired using a high-resolution industrial camera. In the second step, the image undergoes preprocessing, where it is de-noised, and features such as energy, contrast, and variance in multiple orientations and scales are extracted using the Gabor wavelet transform. The third step involves clustering and segmentation of the extracted features to highlight defects. Finally, a decision is made based on the segmented output. Figure 2 shows the block diagram of these steps.

2.1. Gabor wavelets

The Gabor wavelet is a mathematical function used to analyze images in both spatial and frequency domains, filtering images via real parts to extract patterns [26]. In vial defect detection, Gabor wavelets are applied to vial images for feature extraction. The filter scans pixel values in all directions, identifying edge data points by detecting maximum values in gradient intensity matrix, enabling pattern identification and defect detection.

Five factors can affect filtering when using Gabor wavelets. To comprehend this, consider a sine wave overlaid on a two-dimensional Gaussian bell curve. Since it's a two-dimensional bell curve, the sine wave is directional and can possess various orientations, thus influencing the filter with the following factors:

i)   Direction (θ): it indicates the direction of the sine wave
ii)   Offset (φ): indicates the phase offset of the sine wave
iii)   Standard deviation (σ): the smaller the values of this attribute, the closer the values are to the center
iv)   Ellipticity (γ): determines the ellipticity of the 2D image
v)   Wavelength (λ): indicates the distance between the highest points

The wavelets are applied at different orientations and scales. Features such as energy, contrast, and variance are obtained. The output of the Gabor wavelet transformation is a set of feature vectors used in the clustering step for defect detection. Because of the biological relevance of Gabor waves, they are used frequently, and their mathematical properties are defined as in (1):

$$\varphi_{\theta,\omega}(x) = \frac{k_{\theta,\omega}^2}{\sigma^2} \exp\left(-\frac{k_{\theta,\omega}^2 x^2}{2\sigma^2}\right)\left[\exp(ik_{\theta,\omega}) - \exp\left(-\frac{\sigma^2}{2}\right)\right] \tag{1}$$

Where the orientation of the Gabor wavelet and the scale are given by θ and ω respectively, by x = (p, q) representing the spatial domain of the Gabor wavelet $k_{\theta,\omega}$ is the wave vector and is given as in (2):

$$k_{\theta,\omega} = k_\omega \exp(i\theta) \tag{2}$$

where $k_\omega = \frac{k_{max}}{f_v}, k_{max} = \frac{\pi}{2}, f = \sqrt{2}$.

Gabor wavelets are used due to their similarity to the human visual system and because they don't require defect-free samples or threshold settings [10]. They extract image features like edges and points for classification based on spatial, spectral, or texture properties, reducing dimensionality and removing unnecessary data for easier processing. Figure 3 illustrates the application of Gabor wavelets to a 2D image. Figure 3(a) depicts the real wavelets, while Figure 3(b) presents the imaginary wavelets at orientations of 0, π/4, π/2, and 3π/4 radians, and scales ranging from 0.2 to 0.6.
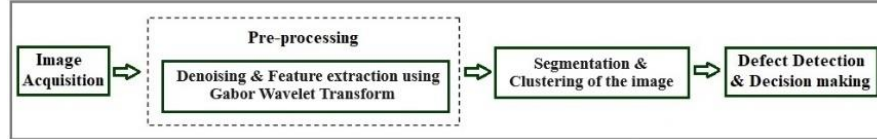

Figure 2. Block diagram of the proposed method

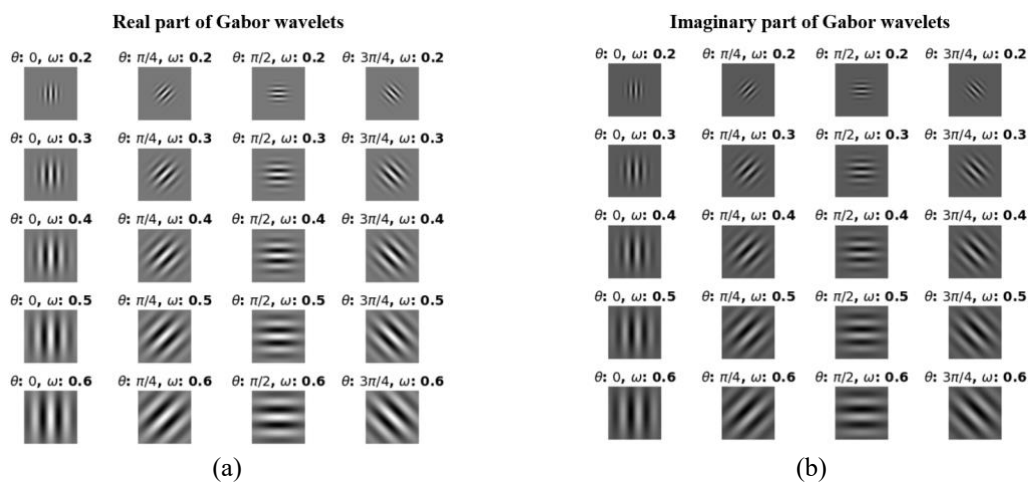(a)   (b)

Figure 3. Gabor wavelets for a 2D image of (a) real wavelets and (b) imaginary wavelets

2.2. K-means clustering

K-means clustering is an unsupervised algorithm that divides data into subgroups called clusters based on characteristics like size, shape, orientation, and scale. The number of clusters (K) is determined

using the Elbow method. K-means minimizes the sum of distances between data points and their nearest centroids, grouping similar data points into clusters without requiring training. The process repeats until no further clustering is possible, ensuring that each dataset belongs to the cluster with the nearest centroid.

2.3. Description of the algorithm

In K-means clustering, the value of K indicates the number of clusters. For instance, if the value of K is set to 2, two clusters will be created; if it is set to 3, three clusters will be created. The formation of K clusters ensures that a dataset is divided into groups based on the similarity of attributes. The K-means clustering algorithm operates as shown in Algorithm 1.

Algorithm 1. K-means clustering
1) Choose the number of K clusters you want to create.
2) Initialize K centroids randomly from the data points.
3) Assign each pixel to the closest centroid on the basis of its Euclidean distance. The Euclidean distance is calculated using the formula given in (3).

$$\text{Euclidean distance} = \sqrt{\sum_{i=1}^{n}(x_i - y_i)^2} \qquad (3)$$

4) Recalculate the centroid as the mean of all pixels assigned to it.
5) Repeat steps 3 and 4 until convergence (when the centroid positions stop changing significantly).
6) Assign each pixel to the cluster to which its centroid belongs.
7) Re-shape the clustered data back into the original image shape.
8) Optionally, apply post-processing to the segmented image (e.g., smoothing or morphological operations).
9) Use the segmented image to detect and classify defects in the vial.

In this process, the input sample is defined as $S = \{p_1, p_2, \ldots, p_m\}$. The variable K denotes the number of clusters, and N signifies the maximum number of repetitions allowed. The output is denoted by $C = \{C_1, C_2, \ldots, C_K\}$. The procedure involves the following steps:

i) From sample S, select randomly k numbers of samples which are initial center vectors of k clusters represented as: $\{\mu_1, \mu_2, \ldots, \mu_k\}$.
ii) For the number n=1, 2, ..., N, apply the following.
a) C is initialized as $C_t = \emptyset \; iijNt = 1, 2, \ldots k$ where C is class division
b) Distance between p_i (for all i=1, 2, ..., m) and every cluster center μ_j (for all j=1, 2, ..., k) is calculated as in (4) and (5).

$$s_{ij} = p_i - \mu_{j2}{}^2 \qquad (4)$$

$$C_{\alpha_i} = C_{\alpha_i} \cup \{p_i\} \qquad (5)$$

For the sample p_i having the smallest distance from μ_j is termed as s_{ij} and its category is represented as α_i, so that the output category is updated as in (6): $C_{\alpha_i} = C_{\alpha_i} \cup \{p_i\}$,

$$\mu_j = \frac{1}{|C_j|}\sum_{p \in C_j} p \qquad (6)$$

c) For the output class C_j, divide all those sample points by (4) for all j=1, 2, 3...., k to obtain the new cluster centers as in (7).

$$\mu_j = \frac{1}{|C_j|}\sum_{p \in C_j} p \qquad (7)$$

d) Repeat step (c) for all k samples.
   Now for p_i the smallest distance from the center of the cluster center is marked as s_{ij} whose category is given by α_i, with this update output as in (8): $C_{\alpha_i} = C_{\alpha_i} \cup \{p_i\}$

$$\mu_j = \frac{1}{|C_j|}\sum_{p \in C_j} p \qquad (8)$$

iii) The procedure is repeated for all the values of j=1, 2, 3...., k for all the values of the k samples, the center vectors of the group have not changed, and the final class division output $C = \{C_1, C_2, \ldots, C_K\}$ is obtained.

The success of the K-means algorithm depends on the value of k that we choose. There are various ways to derive an optimal number of clusters. One such way is to use the Elbow method. This method uses within-cluster sum of squares (WCSS) to get the optimal number of clusters. WCSS is defined as in (9):

$$\sum P_{i \text{ in Cluster1}} \text{ distance}(P_i C_1)^2 + \sum P_{i \text{ in Cluster2}} \text{ distance}(P_i C_2)^2 +$$
$$\sum P_{i \text{ in Cluster3}} \text{ distance}(P_i C_3)^2 \tag{9}$$

3. RESULTS AND DISCUSSION

Dataset description, the study uses a custom-curated dataset specifically designed for vial defect inspection, addressing limitations of publicly available datasets, as noted by Hu *et al*. [24]. This tailored dataset enhances defect detection accuracy by closely reflecting real-world scenarios. Augmentation techniques like rotation and scaling expanded the dataset, while rigorous validation ensured robustness without traditional training.

The image acquisition setup as shown in Figure 4 includes a Nebula LED backlight (Nebula-80R) for adjustable brightness, a Tamron machine vision camera (5 MP, VCXG-52MR) with a 50 mm Baumer lens (M118FM50), and a conveyor system. Figure 4(a) shows the camera positioned to capture the vial surface region, while Figure 4(b) illustrates the camera setup for capturing the vial bottom region. Figure 4(c) depicts the vial placed with the backlight for image acquisition. The computer features a 2.8 GHz 5th gen core i5 processor, 8 GB RAM, Nvidia RTX 3070 GPU, and 1 TB storage. This configuration supports precise image capture and effective defect detection.

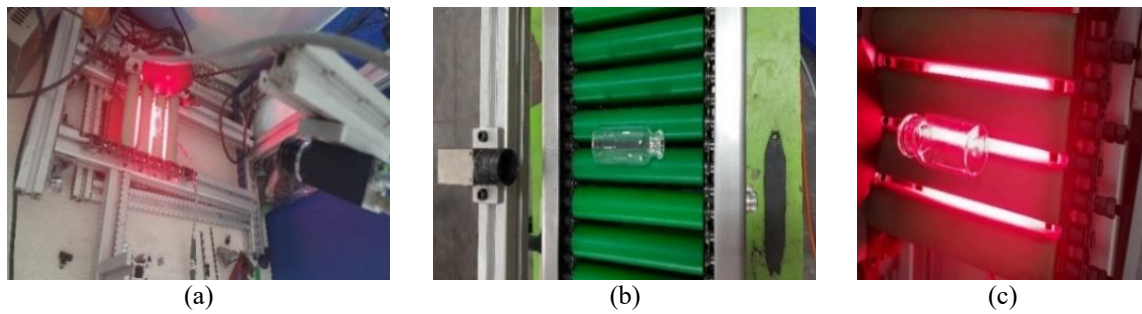| (a) | (b) | (c) |

Figure 4. System setup for image acquisition of (a) camera positioned for capturing vial surface region, (b) camera positioned for capturing vial bottom region, and (c) vial placed with backlight for image acquisition

The study uses vials with defects such as black spots, dust, scratches, dents, bubbles, mouth cracks, neck cracks, and mouth and rim chipping. Most of these defects are caused during the vial manufacturing process. To demonstrate the algorithm, a sample vial image with a mouth crack as a defect is taken, as shown in Figure 5. The resultant images of the vial after the application of Gabor wavelets with a kernel size of 256×256 are shown in Figure 6. Figure 6(a) depicts the real wavelet response, while Figure 6(b) shows the imaginary wavelet response. In both subfigures, the orientations are 0, $\pi/4$, $\pi/2$, and $3\pi/4$ radians from left to right and the different scales are 0.2, 0.3, 0.4, 0.5, and 0.6 from top to bottom.

The Elbow method involves executing K-means clustering on the dataset for K values ranging from 1 to 10, followed by calculating the WCSS for each K value. A curve is then plotted between the calculated WCSS values and the corresponding K values. The optimal K for clustering is determined by identifying the sharp bend, or "Elbow," in the plotted curve, which indicates the point at which adding more clusters does not significantly improve the model's performance.

The image with scratches in the bottom (or base) region undergoes noise removal and feature extraction using Gabor wavelets, as illustrated in Figure 7. Figure 7(a) shows the input image with scratches in the bottom region. Figure 7(b) presents the processed image after feature extraction, where features such as energy, contrast, and variance are extracted. A Gabor wavelet kernel size of 32 captures features at multiple scales, while 16 orientations enhance defect detection from various angles. The image is then segmented using K-means clustering with k=3 clusters, as shown in Figure 7(c). This partitioning distinguishes actual defects from noise. Although increasing the number of clusters could improve segmentation, it also raises computational complexity. Therefore, selecting an optimal k value is crucial for balancing efficiency and data variation capture. Finally, the Canny edge operator is applied to highlight defects in the segmented vial image, as depicted in Figure 7(d).
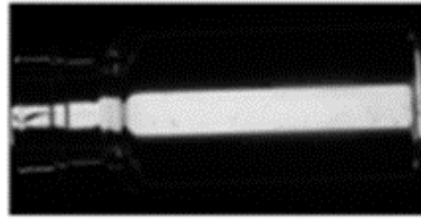
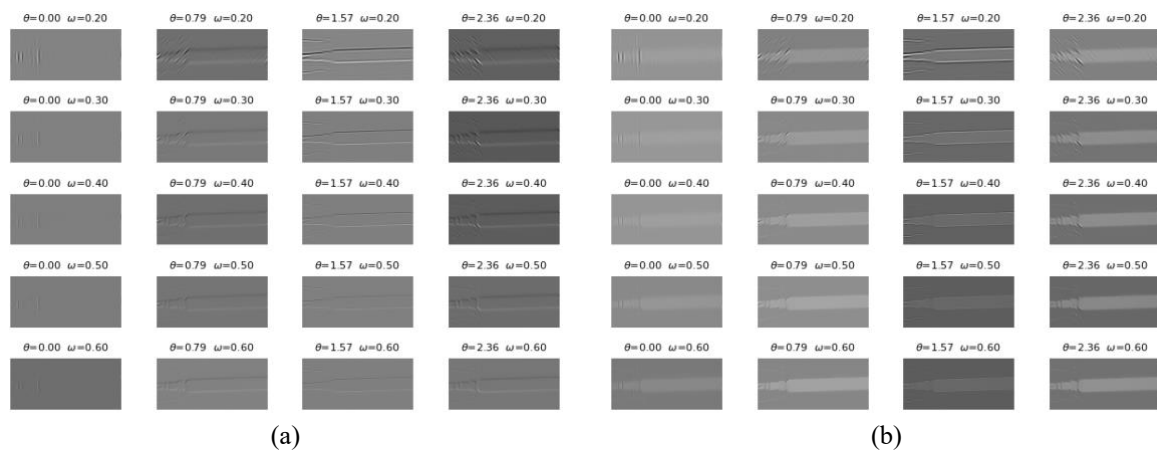Figure 5. A sample vial image with a mouth crack defect

(a)   (b)

Figure 6. Resulting vial images after applying Gabor wavelets of (a) real and (b) imaginary

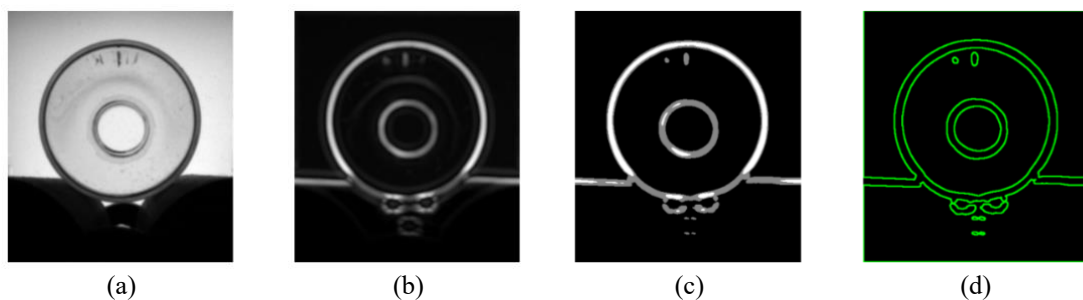(a)   (b)   (c)   (d)

Figure 7. Stepwise processing of a vial image with scratches in the bottom region of (a) input image with scratches in the bottom region, (b) denoising and feature extraction using Gabor wavelet, (c) segmented image using K-means, and (d) identified cluster edges in the output image

The proposed method inspects various defects commonly found in pharmaceutical vials to ensure comprehensive quality assessment. A total of 254 defective vials were analyzed, encompassing a diverse range of defects, including black spots (35 occurrences), cracks (60 occurrences), scratches (80 occurrences), chippings (65 occurrences), as well as other less frequent defects such as bubbles (10 occurrences) and miscellaneous types like flat slim rings, dents, and others (4 occurrences). This dataset allows for a thorough examination of defect detection capabilities across different categories.

The algorithms implemented exhibit varying time and space complexities. Canny edge detection operates in $O(N)$ time, where N is the number of pixels, while the Gabor wavelet and K-means clustering exhibit time complexities of $O(N.k^2.F)$ and $O(n.k.I.d)$ respectively, where F represents the number of Gabor filters, I denotes the number of iterations, and d signifies the number of dimensions. The space complexities for most operations are $O(N)$, except for K-means clustering, which has a space complexity of $O(n.d)$, where d is the number of dimensions. The performance of the implemented system is evaluated using a confusion matrix, which is one of the popular measures used for the analysis of performance parameters such as recall, precision, accuracy, and F1-score. Performance parameters are computed using terminologies such as true positive (TP), true negative (TN), false positive (FP), and false negative (FN).

Figure 8 presents the confusion matrix summarizing the experimental results. The recall, precision, accuracy, and F1-score can be calculated as in (10) to (15).

$$Recall = \frac{True\ Positive}{True\ Positive + False\ Negative} \tag{10}$$

$$Precision = \frac{True\ Positive}{True\ Positive + False\ Positive} \tag{11}$$

$$Accuracy = \frac{True\ Positive + True\ Negative}{Total\ Sample} \tag{12}$$

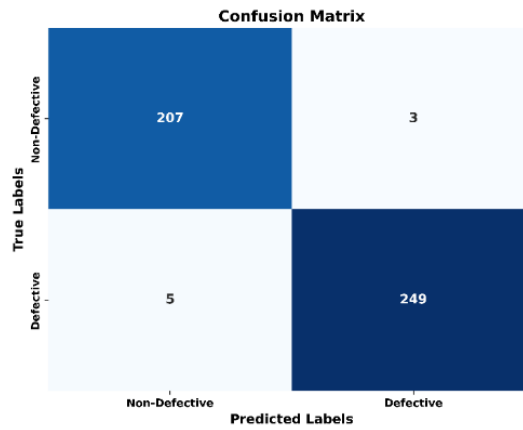$$F1 - score = 2 \times \frac{Precision * Recall}{Precision + Recal} \tag{13}$$

Figure 8. Confusion matrix of experimental results

The area under the curve-receiver operating characteristic (AUC-ROC) curve and the AUC the precision-recall (PR) curve are common metrics used to evaluate the performance of binary classification models as given in (14) and (15).

$$AUC\_ROC = \int_0^1 TPR\big(FPR^{-1}(k)\big)dk \tag{14}$$

$$AUC\_PR = \int_0^1 Precision(k) \cdot \Delta Recall(k)dk \tag{15}$$

Where K represents the number of clusters. The AUC-ROC is calculated considering the TP rate (sensitivity) and the FP rate. The TP rate would represent the proportion of correctly identified defective vials, whereas the FP rate would represent the proportion of non-defective vials incorrectly identified as defective. The AUC-PR measures the balance between precision and recall. Precision would represent the accuracy of the identification of the defect among all the vials identified as defective, while recall (or sensitivity) would represent the proportion of actual defective vials correctly identified. The proposed method has produced 98.81% recall, 98.03% precision, 98.28% accuracy, and the F1-score obtained is 98.42%. The AUC-ROC and AUC-PR values obtained are 98.30 and 98.96%, respectively, when the value of k is set to 3 and is shown in Figure 9.

The performance of the proposed methodology across various segmentation settings is assessed by integrating different k values, as shown in Figure 10. Figure 10(a) presents the ROC curve, while Figure 10(b) illustrates the PR curve for different k values. The analysis reveals that varying K impacts model performance, with K=3 yielding optimal sensitivity, specificity, precision, and recall. This indicates that defect detection is most effective when K is set to 3, highlighting the importance of selecting an appropriate K value for superior performance.

The proposed method for vial defect detection takes an average computational time of around 355 microseconds for all types of defects, and suggests a relatively efficient processing speed. The comparison of various techniques or methodologies and the one used in this study is given in Table 1, which provides empirical evidence that demonstrates the superior performance of the proposed method compared to alternative defect detection algorithms. The paper presents results from comparative experiments that highlight the method's higher accuracy. Overall, the preference for the proposed method using Gabor wavelet clustering and K-means clustering is justified by its ability to effectively extract relevant features that

distinguish between defective and non-defective regions of vials. The graph of the comparison of accuracy across different methods is shown in Figure 11.
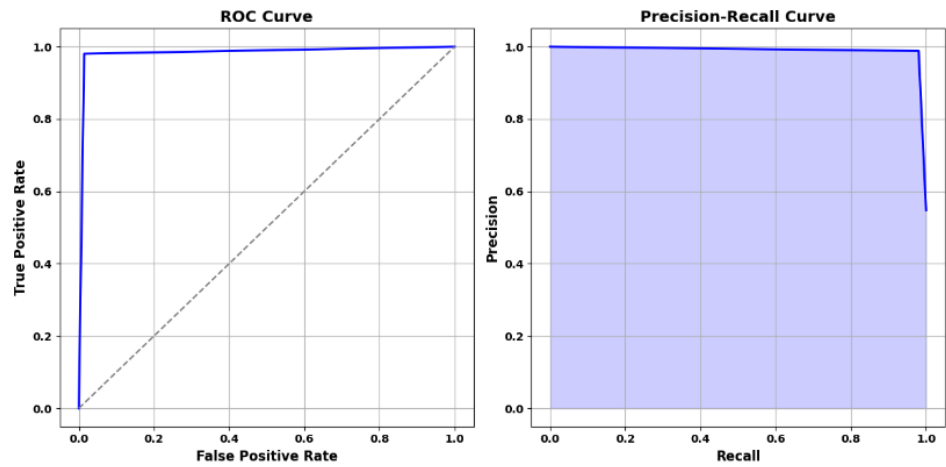

Figure 9. The AUC-ROC and AUC-PR curves

(a)   (b)
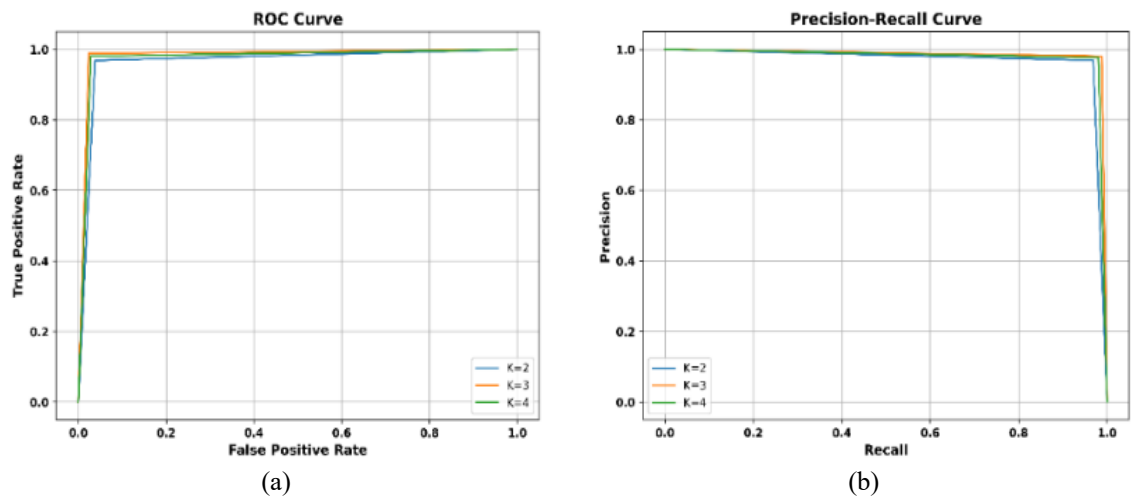
Figure 10. Performance evaluation metrics of (a) receiver operating characteristic curve and
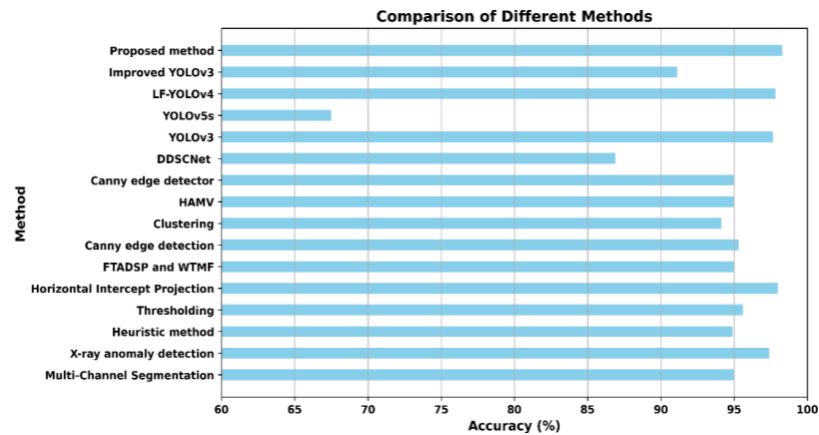(b) precision-recall curve

Figure 11. Comparison of precision across different methods

Table 1. The performance of various methods

Sl. No.	Methodology	Accuracy (%)
1	Multi-channel segmentation [1]	95
2	X-ray anomaly detection [2]	97.4
3	Heuristic method [3]	94.9
4	Thresholding [4]	95.6
5	Horizontal intercept projection [5]	98
6	FTADSP and WTMF [6]	95.00
7	Canny edge detection [7]	95.33 (avg)
8	Clustering [8]	94.12
9	HAMV [9]	95.00
10	Canny edge detector [10]	95.00
11	DDSCNet [15]	86.9 (highest)
12	YOLOv3 [16]	97.66
13	YOLOv5s [17]	67.5
14	LF-YOLOv4 [18]	97.83
15	Improved YOLOv3 [19]	91.12
16	Proposed method	98.28

4. CONCLUSION

This study adopts a novel approach by focusing on the development and evaluation of an algorithm for defect detection in vials. The algorithm is designed to analyze individual vial images to identify and localize the presence of defects, without training a model for vial classification. Gabor wavelets are a powerful tool in image processing that can be used to detect defects in vials by extracting meaningful features from the image data. Combining Gabor wavelets with clustering of K-means enables accurate and efficient detection of defective vials, utilizing features such as energy, contrast, and variance for superior results. Robust to variations in illumination, orientation, and scale, Gabor wavelets ensure reliability across diverse manufacturing environments. Unlike predefined models, K-means clustering adapts to varying characteristics, operates in an unsupervised manner, and accommodates changes in manufacturing processes or product specifications. This holistic approach enhances the method's ability to identify various types of defects, including subtle anomalies that may be challenging to detect using traditional algorithms. With an average computational time of 355 microseconds, the proposed method demonstrates the potential for real-time defect detection, detecting scratches, dents, black spots, chipping, cracks, and more. Comparative analysis indicates better accuracy in all regions of the vial tested for defects, highlighting the method's potential for adoption in the pharmaceutical industry. The method described operates on individual vial images sequentially. For high-throughput manufacturing environments, where multiple vials are inspected simultaneously, this approach may not be scalable. Future research could investigate parallel processing or batch inspection techniques to improve throughput and aim at exploring the integration of optimized ML algorithms, such as CNNs, SVMs, random forests, and deep learning methods such as R-CNNs, U-Net, and GANs, to improve automated defect classification.

AUTHOR CONTRIBUTIONS STATEMENT

This journal uses the Contributor Roles Taxonomy (CRediT) to recognize individual author contributions, reduce authorship disputes, and facilitate collaboration.

Name of Author	C	M	So	Va	Fo	I	R	D	O	E	Vi	Su	P	Fu
Vishwanatha C. R.	✓	✓	✓		✓	✓	✓	✓	✓	✓				
V. Asha	✓	✓		✓					✓	✓	✓	✓	✓	
Channabasava	✓		✓		✓		✓			✓				
Sreekanth Rallapalli		✓		✓		✓				✓			✓	

C	:	**C**onceptualization	I	:	**I**nvestigation	Vi	:	**Vi**sualization
M	:	**M**ethodology	R	:	**R**esources	Su	:	**Su**pervision
So	:	**So**ftware	D	:	**D**ata Curation	P	:	**P**roject administration
Va	:	**Va**lidation	O	:	Writing - **O**riginal Draft	Fu	:	**Fu**nding acquisition
Fo	:	**Fo**rmal analysis	E	:	Writing - Review & **E**diting			

CONFLICT OF INTEREST STATEMENT
The authors declare no conflict of interest.

DATA AVAILABILITY
The data that support the findings of this study are available from the first author [VCR], upon reasonable request.

REFERENCES

[1]   B. Chen, C. Li, P. Yuan, Y. Yan, and Y. Yin, "Research on defect detection of bottle cap interior based on low-angle and large divergence angle vision system," *PLoS ONE*, vol. 19, no. 5, May, 2024, doi: 10.1371/journal.pone.0303744.
[2]   J. Rapcewicz and M. Malesa, "Active learning in feature extraction for glass-in-glass detection," *Electronics* vol. 13, no. 11, 2024, doi: 10.3390/electronics13112049.
[3]   M. Eshkevari, M. J. Rezaee, M. Zarinbal, and H. Izadbakhsh, "Automatic dimensional defect detection for glass vials based on machine vision: a heuristic segmentation method," *Journal of Manufacturing Processes*, vol. 68, pp. 973–989, 2021, doi: 10.1016/j.jmapro.2021.06.018.
[4]   O. Farhangi, E. Sheidaee, and A. Kisalaei, "Machine vision for detecting defects in liquid bottles: an industrial application for food and packaging sector," *Cloud Computing and Data Science*, pp. 242–254, 2024, doi: 10.37256/ccds.5220244756.
[5]   X. Liu, Q. Zhu, Y. Wang, X. Zhou, K. Li, and X. Liu, "Machine vision based defect detection system for oral liquid vial," *2018 13th World Congress on Intelligent Control and Automation (WCICA)*, pp. 945–950, 2018, doi: 10.1109/WCICA.2018.8630441.
[6]   X. Zhou *et al.*, "A surface defect detection framework for glass bottle bottom using visual attention model and wavelet transform," *IEEE Transactions on Industrial Informatics*, vol. 16, no. 4, pp. 2189–2201, 2020, doi: 10.1109/TII.2019.2935153.
[7]   L. Fu, S. Zhang, Y. Gong, and Q. Huang, "Medicine glass bottle defect detection based on machine vision," in *2019 Chinese Control and Decision Conference (CCDC)*, 2019, pp. 5681–5685, doi: 10.1109/CCDC.2019.8832688.
[8]   R. Kulkarni, S. Kulkarni, S. Dabhane, N. Lele, and R. S. Paswan, "An automated computer vision-based system for bottle cap fitting inspection," *2019 Twelfth International Conference on Contemporary Computing (IC3)*, Noida, India, 2019, pp. 1-5, doi: 10.1109/IC3.2019.8844942.
[9]   C. He, C. Li, B. Chen, B. Yuan, and Y. Yin, "Research on defect detection of the outer side of bottle cap based on high angle and multi-view vision system," *IEEE Access*, vol. 11, pp. 65798–65809, 2023, doi: 10.1109/ACCESS.2023.3290616.
[10]   M. Kazmi, B. Hafeez, H. R. Khan, and S. A. Qazi, "Machine-vision-based plastic bottle inspection for quality assurance," in *Engineering Proceedings*, 2022, vol. 20, no. 1, doi: 10.3390/engproc2022020009.
[11]   C. Li, Y. Yin, B. Yuan, and X. Li, "Research on surface defect detection technology based on the zonal and time-sharing computational imaging," *IEEE Access*, vol. 10, pp. 79574–79583, 2022, doi: 10.1109/ACCESS.2022.3163726.
[12]   S. B. Jha and R. F. Babiceanu, "Deep CNN-based visual defect detection: survey of current literature," *Computers in Industry*, vol. 148, 2023, doi: 10.1016/j.compind.2023.103911.
[13]   T. A. Korzhebin and A. D. Egorov, "Comparison of combinations of data augmentation methods and transfer learning strategies in image classification used in convolution deep neural networks," *2021 IEEE Conference of Russian Young Researchers in Electrical and Electronic Engineering (ElConRus)*, pp. 479–482, 2021, doi: 10.1109/ElConRus51938.2021.9396724.
[14]   K. Liu, Y. Liu, C. Peng, Y. Chang, and Y. Zhao, "Design of hardware acceleration in edge computing device for bottle cap high-speed inspection," *Wireless Communications and Mobile Computing*, vol. 2022, 2022, doi: 10.1155/2022/5270887.
[15]   H. Xu, Y. Xu, and K. Hu, "A vision-based inspection system for pharmaceutical production line," *Journal of Supercomputing*, vol. 81, no. 4, 2025, doi: 10.1007/s11227-025-07135-8.
[16]   H. Lv, S. Huang, W. Xie, Z. Chen, Z. Guo, and X. Zhang, "Multi-scale based defect detection for automotive glass," *Journal of Physics: Conference Series*, vol. 2303, no. 1, 2022, doi: 10.1088/1742-6596/2303/1/012068.
[17]   Y. Zhang, S. Shu, X. Lang, H. Liang, Z. Yu, and Z. Yang, "A real-time method for detecting bottom defects of lithium batteries based on an improved YOLOv5 model," *Measurement Science and Technology*, vol. 34, no. 12, 2023, doi: 10.1088/1361-6501/acf9bf.
[18]   X. Chen, Z. Jiang, H. Cheng, H. Zheng, and Y. Du, "LF-YOLOv4: a lightweight detection model for enhancing the fusion of image features of surface defects in lithium batteries," *Measurement Science and Technology*, vol. 35, no. 2, 2024, doi: 10.1088/1361-6501/ad0690.
[19]   J. Liu and D. Zhang, "Research on vehicle object detection algorithm based on improved YOLOv3 algorithm," in *Journal of Physics: Conference Series*, 2020, vol. 1575, no. 1, doi: 10.1088/1742-6596/1575/1/012150.
[20]   L. Shen, H. Tao, Y. Ni, Y. Wang, and V. Stojanovic, "Improved YOLOv3 model with feature map cropping for multi-scale road object detection," *Measurement Science and Technology*, vol. 34, no. 4, 2023, doi: 10.1088/1361-6501/acb075.
[21]   Z. Huang, H. Hu, Z. Shen, Y. Zhang, and X. Zhang, "Lightweight edge-attention network for surface-defect detection of rubber seal rings," *Measurement Science and Technology*, vol. 33, no. 8, 2022, doi: 10.1088/1361-6501/ac6663.
[22]   H. Wang, X. Xu, Y. Liu, D. Lu, B. Liang, and Y. Tang, "Real-time defect detection for metal components: a fusion of enhanced canny–devernay and YOLOv6 algorithms," *Applied Sciences*, vol. 13, no. 12, 2023, doi: 10.3390/app13126898.
[23]   M. Stasevych and V. Zvarych, "Innovative robotic technologies and artificial intelligence in pharmacy and medicine: paving the way for the future of health care-a review," *Big Data and Cognitive Computing*, vol. 7, no. 3, Aug. 2023, doi: 10.3390/bdcc7030147.

[24] K. Hu, Z. Chen, H. Kang, and Y. Tang, "3D vision technologies for a self-developed structural external crack damage recognition robot," *Automation in Construction*, vol. 159, 2024, doi: 10.1016/j.autcon.2023.105262.

[25] M. H. Ha, Y. G. Kim, and T. H. Park, "Stain defect classification by gabor filter and dual-stream convolutional neural network," *Applied Sciences*, vol. 13, no. 7, 2023, doi: 10.3390/app13074540.

[26] A. K. Samantaray and A. D. Rahulkar, "Fundamentals of Gabor wavelet filter banks," *Feature Extraction in Medical Image Retrieval*, pp. 41–70, 2024, doi: 10.1007/978-3-031-57279-1_3.

BIOGRAPHIES OF AUTHORS

Dr. Vishwanatha C. R. 🆔 📊 SC ◖ holds a Ph.D. in Computer Applications from Visvesvaraya Technological University, Belagavi, Karnataka, India. He is an Assistant Professor at the Department of Computer Applications, Nitte Meenakshi Institute of Technology, Nitte (Deemed to be University), Bengaluru, India. He specializes in machine vision algorithms. His research interests span image processing, and artificial intelligence, and he has contributed to numerous research articles. His primary research directions include machine vision, machine learning, and automation. He can be contacted at email: vishwanathcr@gmail.com.

Dr. V. Asha 🆔 📊 SC ◖ holds a Ph.D. in Computer Science from the University of Mysore, Karnataka, India. She is a Professor and Head at the Department of Computer Applications, New Horizon College of Engineering, Bengaluru, India. She received her Bachelor's and Master's degrees in Computer Science from Mysore University. Her research interests include image processing, pattern recognition, machine learning, and information science. She has published research articles in various reputed Journals and presented her papers at various national and international conferences. She can be contacted at email: asha.gurudath@gmail.com.

Channabasava 🆔 📊 SC ◖ holds MCA degree from Visvesvaraya University, Belagavi, Karnataka, India. He is an Assistant Professor at the Department of Computer Applications, Nitte Institute of Technology, Bengaluru, India. He specializes in cloud computing, data science, internet of things, machine learning, and natural language processing. He has contributed to the various research articles in machine learning and AI. He can be contacted at email: chan.snd@gmail.com.

Dr. Sreekanth Rallapalli 🆔 📊 SC ◖ holds a Ph.D. in Computer Science from Bharathiar University, Coimbatore, Tamilnadu, India. He is a Professor and Head of Department at the Department of Computer Applications, Nitte Meenakshi Institute of Technology, Bengaluru, India. He specializes in artificial intelligence, machine learning, and big data. His research interests span machine learning, deep learning, and cloud computing. He has contributed to numerous research articles. His primary research directions include big data, artificial intelligence and machine learning. He can be contacted at email: rsreekanth1@yahoo.com.